JOURNAL OF MATERIALS SCIENCE **40** (2005) 3749–3758

Sintering mechanisms in $YBa_2Cu_3O_{7-x}$ superconducting ceramics

E. R. BENAVIDEZ*
Facultad Regional San Nicolás, Universidad Tecnológica Nacional, Colón 332 - (2900) San Nicolás, Argentina
E-mail: ebenavidez@frsn.utn.edu.ar

C. J. R. GONZÁLEZ OLIVER
Centro Atómico Bariloche (CNEA), Av. Bustillo km.9, 5-(8400) Bariloche, Argentina; C. O. N. I. C. E. T
E-mail: gon@cab.cnea.gov.ar

The densification of ceramic compacts of $YBa_2Cu_3O_{7-x}$ (123) was studied with a vertical dilatometer. The runs effected under isothermal conditions (ISO) covered the 920–970°C range and were performed under static air atmosphere. Also, controlled heating rate (CHR) runs, from about 800 to 1050°C, were conducted at 5°C/min under either flowing oxygen or static air. The ISO data could be satisfactorily fitted by the solution-precipitation (SP) model giving an activation enthalpy of 221 kJ/mol. Furthermore, the CHR data for 920–970°C was also fitted with the same model giving 207 kJ/mol as the activation energy. From analysis of CHR data, the initial stage sintering is driven by solid state sintering between 827–894°C (823–908°C in O_2). Then, in the interval 902–920°C (914–934°C in O_2) the intermediate stage driven by grain growth (GG), competes with the rearrangement process associated to the presence of a liquid phase. This last process applied because the next sintering stage in the range 922–970°C (938–990°C in O_2 flow) could be fitted by the SP model with an activation enthalpy of 207 kJ/mol (229 kJ/mol in O_2). In the range 972–995°C (990–1014°C in O_2), the solid state (GG) intermediate stage mechanism and/or viscous flow competes with the SP process.

1. Introduction

A great deal of physical properties in ceramic materials depend on the sintering process. Knowledge of the mechanisms controlling the sintering process can be very relevant to control for example the final relative density (ρ_r) and grain size of the ceramic body. The evolution of the density with temperature increasing or with time increasing, for isothermal conditions, determine the kinetics of the sintering. Dilatometry, whereby a characteristic linear dimension of the specimen is continuously measured, is one of the most important methods to estimate such kinetics.

Several sintering studies were effected on $YBa_2Cu_3O_{7-x}$ (123) ceramics, where densification properties [1–3], and liquid phases [4–7] and grain growth [8–12] effects on the microstructural development of 123 were analyzed. When liquid phases are present increased densifications and grain growth rates [5, 7, 9] are usually measured. These generally non-superconducting crystallized liquids are situated on the 123 grain boundaries [4, 5] reducing the effective area of contact among 123 grains, and degrading the electric transport properties. Although the Jc is the main property that permit to judge the quality of a superconducting material, a concrete relationship between for instance the grain size and critical current density (Jc) [8], has not been found yet. According to [13] a high percentage of porosity in the 123 superconductor results in low Jc values due to a weak connectivity in between the superconducting grains. On the contrary, for low percentages of porosity the superconductor may also exhibit low Jc values owing to a decreased oxygenation of the 123 grains. That is, the lack of connectivity among the pores, for low porosity bodies, does not allow rapid oxygen diffusion towards the 123 grains. An optimal density $90 \pm 5\%$ of the theoretical density has been postulated in [14].

In previous investigations [15, 16] on systems 123 and 123 + Ag, the dilatometer densification regimes for $T <$ Tp (Tp: Peritectic temperature) were found to depend strongly on the oxygen partial pressure (pO_2) in the sintering atmosphere. For a given pO_2, the peritectic decomposition kinetics for $T \geq$ Tp, also studied with the dilatometer, was very different for 123 + Ag compared to that for pure 123. The much slower

*Author to whom all correspondence should be addressed.

decomposition rates obtained for 123 + Ag suggested a very different peritectic liquid for 123 + Ag as compared to that for 123. From the densification analysis in the range ~960°C to Tp, using viscous flow or creep densification models, it was found the apparent activation enthalpy (ΔH) for 123 + Ag was smaller than that for 123. Recently, there were also analyzed the solidification behavior of $YBa_2Cu_3O_{7-x}$ ceramics cooled from Tp [17], and, the densification, $T <$ Tp, and peritectic decomposition, $T \geq$ Tp, of $YBa_{2-x}Sr_xCu_3O_{7-\delta}$ (YBSCO) ceramics [18].

In this work the sintering kinetics of 123 alone is studied from ~820°C to Tp (1040°C in O_2, 1020°C in air), attempting to identify the main densification mechanisms operating in the different temperature ranges where strong changes in densification rates were measured. The green 123 compacts, with initial relative densities $\rho_r \approx 0.60$, were analyzed at constant temperatures in the range 910 to 970°C in air, and at controlled heating rate (in air and oxygen atmospheres) in the range from about 820°C to Tp.

2. Experimental and densification models

2.1. Preparation and characterization of samples

Powder of $YBa_2Cu_3O_{7-x}$ (particle size in the 1–5 μm range) was supplied by Seattle Specialty Ceramics Inc. This powder was mixed mechanically adding 1 wt% of polyvinyl butyral (PVB, MW ~ 150.000) as binder. Previously, the PVB was dissolved in isopropyl alcohol. The coated 123-ceramic particles were pressed uniaxially at 100 MPa in a cylindrical matrix. Typical dimension of the pellets were 8.1 mm in diameter and 2 mm in height, and their green densities were estimated from the geometrical volume and weight.

Prior to the dilatometric runs, the pellets were heated at 750°C during 4 h under a flow of oxygen, after which no dimensional changes were detected.

The shrinkage of 123 compacts was monitored in a vertical dilatometer (Theta Instruments Inc., Dilatronic II) used in differential form. The runs were effected at constant heating rates (CHR) of 5°C/min in static air ($pO_2 = 0.21$ atm) and in flowing oxygen ($pO_2 = 1$ atm) atmospheres. The isothermal treatments (ISO) were effected in static air, and these ISO runs consisted on heating the compacts at 5°C/min up to the selected temperature, which was maintained constant (±2°C) during the isothermal cycle. One group of runs was performed with the pushrod applying a slight pressure throughout the dilatometric run (named: free sintering, 0 kPa). Other group of dilatometries was performed with the pushrod applying 10 g additional load on the sample (called: load sintering). The load was regulated by the counterweight system of the dilatometer. According to the area (12.9 mm^2 = 1/4 original area of sample) of the compact exposed to the pushrod, the constant pressure exerted during the load dilatometric cycle was 8 kPa. Between the sample and the end of the alumina pushrod, a Mg-stabilized ZrO_2 sheet (ZrO_2-Mg) 0.2 mm in thickness was placed to prevent chemical reaction between the 123 pellet and the alumina pushrod. Besides, the sheet allowed the pushrod to exert an uniform pressure on the sample. A similar sheet was placed below the 123 sample to avoid sticking to the alumina holder bottom plate of the dilatometer. Silica glass was used as a reference material and it was placed between two ZrO_2-Mg sheets of 0.2 mm in thickness as for the 123 samples. It should be noted the densification or shrinkage relative values ($\Delta L/Lo$) are taken as positive values defined as $\Delta L/Lo = [Lo - L(T,t)]/Lo$, where Lo is the initial height of the pellet and $L(T,t)$ is the instantaneous height of the sample either at temperature T (for CHR) or after time t for isothermal densification (ISO); for the latter case Lo corresponds to the sample-height for $t = 0$.

Thermal evolution of 123 powders, in air or oxygen atmospheres, was examined by differential thermal analysis (DTA) and thermogravimetric (TG) measurements using a Netzsch STA-409 apparatus. The heating conditions were similar to those for the dilatometric essays.

Some pellets were heated at 5°C/min up to temperatures in the range 900–1000°C and then, they were quenched by quick removal from the furnace and dropping into liquid nitrogen. These samples were embedded in acrylic resin and polished with diamond paste down to 1 μm particle size. The microstructure of these samples was observed by SEM using a Philips 515 microscope.

2.2. Theoretical models

In this work are adopted theoretical models like those corresponding to the initial and intermediate stage of sintering by solid state diffusion (SSS), liquid phase sintering (LPS), and viscous flow densification (VF). In the models: γ, Ω, G, D and c are, respectively, surface energy, vacancy volume, grain size, the diffusion coefficient, and the heating rate. Also are used the linear shrinkage of the compact $\Delta L/Lo$, and the rate of the linear shrinkage $d(\Delta L/Lo)/dT$. The derivative curve was smoothed by averaging each original data point i in the interval $[i-5, i+5]$. The diffusion coefficient was approximated as: $D = Do.\exp(-Q/RT)$, where Q is the activation energy corresponding to the diffusion mechanism. Hence, the linear zones of ln[function $(\Delta L/Lo, d(\Delta L/Lo)/dT, T)$] versus $(1/T)$ plots will have a slope $-Q/R$. All fits were obtained using linear least squares analysis. The magnitude of [function $(\Delta L/Lo, d(\Delta L/Lo)/dT, T)$] is given explicitly in the left hand side of the following Equations 1, 2, 3, 4, 5a, 5b and 6.

For the *initial stage* of sintering, a model developed by Young and Cutler [19] was used, such as when the *grain boundary diffusion* is the main mechanism of densification, the relationship between the linear shrinkage, the rate of shrinkage, and the absolute temperature is given by Equation 1:

$$\ln[T \cdot (\Delta L/Lo)^{2.06} \cdot d(\Delta L/Lo)/dT] = \ln\left(K_B^{\text{ini}}\right) - Q_B^{\text{ini}}/R.T \quad (1)$$

Where: $K_B^{\text{ini}} = 11.\gamma.\Omega.\delta.Do_B/(k.c.G^4)$, and $D_B = Do_B.\exp(-Q_B^{\text{ini}}/R.T)$ is the grain boundary diffusion coefficient.

The superscript 'ini' indicates the initial sintering stage (ini: initial) and the subscript 'B' indicates the grain boundary diffusion mechanism (B: grain boundary).

On the other hand, if *volume or lattice diffusion* is the main diffusion mechanism, it is proposed the Equation 2:

$$\ln[T\cdot(\Delta L/Lo)^{1.03}\cdot d(\Delta L/Lo)/dT] = \ln\left(K_V^{\text{ini}}\right) - Q_V^{\text{ini}}/R.T \quad (2)$$

where: $K_V^{\text{ini}} = 21.\gamma.\Omega.\ \text{Do}_V/(\text{k.c.G}^3)$, and $D_V = Do_V.\exp(-Q_V^{\text{ini}}/R.T)$ is the volume diffusion coefficient.

The intermediate stage of sintering by solid state reaction (densification asociated to grain growth) was modeled by Coble [20] who presented several equations describing removal of porosity corresponding to volume and grain boundary diffusions. These equations were corrected by Coble [21] and Coble and Gupta [22] in subsequent revisions. This model was adapted to CHR densification assuming negligible grain growth by Genuist and Haussonne [23]. If the control mechanism of sintering is *grain boundary diffusion*, the following expression (Equation 3) is obtained:

$$\ln\{T\cdot(1-\Delta L/Lo)^{-4}\cdot d(\Delta L/Lo)/dT\cdot[1-(Lf/Lo)^3/(1-\Delta L/Lo)^3]^{1/2}\} = \ln\left(K_B^{\text{int}}\right) - Q_B^{\text{int}}/RT \quad (3)$$

where: $K_B^{\text{int}} = 860.\delta.Do_B.\gamma.\Omega.(Lo/Lf)^3/(3.k.c.G^4)$, and Lf is the length of the densified sample.

In this work the green density (ρ_o) of the prefired ceramic compacts was about 60% of the theoretical density ($\rho_t = 6.38$ g/cm^3). Considering $\rho_f = \rho_t$ and using [24] the relation $\rho = (Lf/L)^3.\rho_f$, if $\rho_o = 0.60$ and $\rho_f = (Lf/Lo)^3\rho_f$, then $Lf/Lo = 0.843$. In this way to attain theoretical density for 123, the compact must shrink in isotropic way an amount $(Lf-Lo)/Lo = 0.843-1 = -0.157$, i.e. the theoretical total shrinkage is 15.7%. When the mechanism controlling the intermediate stage in densification is *volume diffusion*, the following equation applies:

$$\ln[T\cdot(1-\Delta L/Lo)^{-4}\cdot d(\Delta L/Lo)/dT] = \ln\left(K_V^{\text{int}}\right) - Q_V^{\text{int}}/RT \quad (4)$$

where $K_V^{\text{int}} = 335.Do_V.\gamma.\Omega.(Lo/Lf)^3/(3.k.c.G^3)$.

The densification via *viscous sintering* (Frenkel's theory [25]) was adapted to the analysis of CHR data by Cutler [26], and the following expression results:

$$\ln[d(\Delta L/Lo)/dT] = \ln(K_{\text{fv}}) - Q_{\text{fv}}/RT \quad (5a)$$

with $K_{\text{fv}} = \gamma/(G.c.\eta_o)$, with η_o being the preexponencial factor in the viscosity expression: $\eta = \eta_o.\exp(+Q/RT)$.

Equation 5a can also be used to describe the *rearrangement* process of grain-agglomerates by liquid phase sintering according to Kingery's model [27]. This stage is characterized by the formation of a liquid phase which wets the main particles, forming liquid necks between them. These necks join the particles together by capillary pressure producing some densification. It turns out a similar expression to that for viscous sintering:

$$\ln[d(\Delta L/Lo)/dT] = \ln\left(K_L^{\text{rea}}\right) - Q_L^{\text{rea}}/RT \quad (5b)$$

Finally, following Kingery's model [25], the solution-precipitation process was adapted by González Oliver *et al.* [28] to CHR densification, obtaining:

$$\ln[T\cdot(\Delta L/Lo)^2\cdot d(\Delta L/Lo)/dT] = \ln\left(K_L^{\text{sp}}\right) - Q_L^{\text{sp}}/R.T \quad (6)$$

with: $K_L^{\text{sp}} = 32.k_1.\delta.D_o.C_o.\gamma_{1v}.\Omega/(k_2.R.c.G^4)$, where: k_1 and k_2 are geometrical constants and Co is the initial solubility of the solid in the liquid. The superscript is assigned to stage (rea: rearrangement, SP: solution-precipitation) developing in the liquid phase sintering (subscript L).

3. Results

Before densification, thermal expansion behavior of ceramic pellets (not shown here) is stopped at 725°C (or 755°C in O_2). The expansion is interrupted because the compact starts the densification process. The onset of the samples contraction was at 737°C in air and at 767°C in O_2. Therefore, in the following analysis of the densification behavior, Lo corresponds to the length of the compact at $To = 730$°C in air (or $To = 760$°C in O_2), i.e. Lo is the length of the sample just prior to the beginning of the shrinkage process. At these temperatures, according to Mizusaki *et al.* [29], the crystalline structure of $YBa_2Cu_3O_{7-x}$ in both atmospheres is tetragonal.

3.1. Controlled heating rate (CHR) sintering

In Fig. 1 are shown the densification curves of 123 compacts, free and load sintering, heated in air. As noted in Section 2.2, ΔL/Lo is taken as positive. Densification rates in Figs 1 and 2 are given in units of 10^{-3}/°C. At the bottom part of Fig. 1 are shown the DTA and TG curves of 123 powders.

The compacts accelerate their densification process from 910°C coinciding with the first endothermic peak detected in the DTA curve at 911°C, to which is associated a mass loss of 0.07% respect to the initial mass (m_O). A second endothermic peak appears at 927°C. The first peak is associated to the eutectic reaction (Equation 7) in the Y_2O_3-BaO-CuO system [30–32]:

$$YBa_2Cu_3O_{7-x} + BaCuO_2 + CuO \rightarrow L(e1) \quad (7)$$

During reaction (7) the eutectic liquid L(e1), rich in barium and cooper, is generated. The second peak

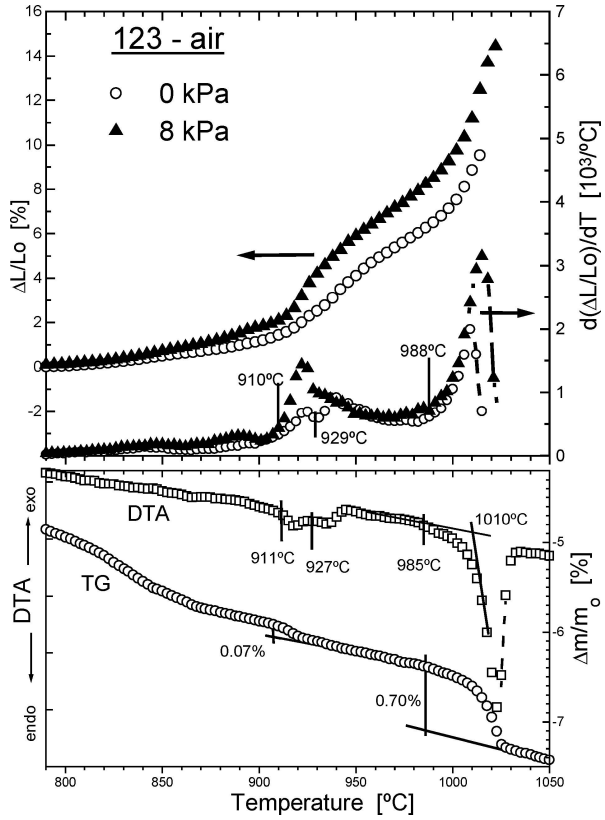

Figure 1 Absolute linear densification and contraction rate curves of 123 compacts in air. At the bottom are shown the DTA/TG curves of 123 powder heated under similar conditions as for the above compacts.

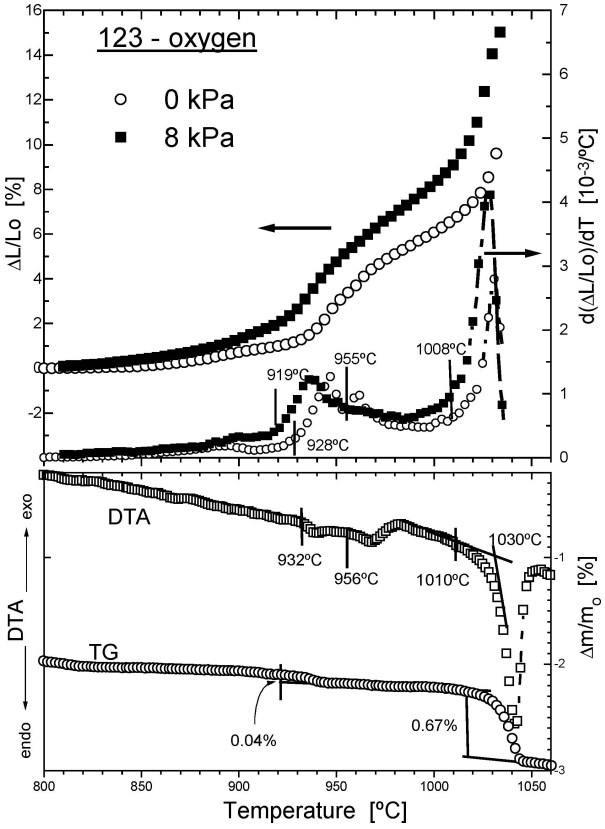

Figure 2 Dilatometric and contraction rate curves of 123 compacts in oxygen. At the bottom part, the DTA/TG curves of 123 powder heated under similar conditions to that for the compacts are shown.

is more conflictive in respect to its identification but it could be associated to the binary eutectic reaction [30–32]:

$$BaCuO_2 + CuO \rightarrow L(e2) \qquad (8)$$

The liquid L(e2) generated in this reaction is also rich in Ba and Cu.

From 988°C the contraction curve is accelerated again coinciding with the temperature (985°C) where the DTA-curve deviates from its base line indicating the beginning of the peritectic decomposition or melting process of 123 [30–32]:

$$YBa_2Cu_3O_{7-x} \rightarrow Y_2BaCuO_5 + L(p1) \qquad (9)$$

According to the DTA-curve, the T_{onset} corresponding to peritectic decomposition of 123 is 1010°C, and the loss mass during this reaction is $\Delta m/m_o = 0.70\%$. At 1015°C (taken as Tp) the contraction curve deflects to a constant value; at this temperature (Tp) the maximum contraction ΔL/Lo reaches 14.5%.

The shrinkage curve under $pO_2 = 1$ atm is shown in Fig. 2. This curve presents a similar behavior to that shown in Fig. 1, but in this case there is a shift of around 20–30°C towards higher temperatures. The e1-reaction (Equation 7) is detected at 932°C at which temperature there is an increase in the densification rate. Under pure oxygen atmosphere the second endothermic reaction starts at about 956°C.

The partial fusion or decomposition of 123 in O_2 is obtained now at $T_{onset} = 1030$°C. It is observed that at 1010°C the DTA-curve departs from its baseline and this coincides with the temperature corresponding to the increase in densification rate as it is seen in the d(ΔL/Lo)/dT curve at 1008°C. The shrinkage attains its maximum value $\Delta L/Lo = 15.1\%$ at 1036°C for the present case involving heatings under oxygen flow.

The following may be noted in relation to possible explanations of the densification regimes detected in these CHR curves. The first levels of contractions in Figs 1 and 2 are fitted by models applied to the initial stage sintering, Equations 1 and 2. In Fig. 3 are shown the curves obtained from both equations applied to the first 3.5% in linear shrinkage. In this figure the value of n in y-axis is $n = 2.06$ (Equation 1, grain boundary diffusion), and $n = 1.03$ (Equation 2, volume diffusion). According to these graphics, two temperature intervals can be fitted by straight lines (solid straight lines in Fig. 3).

In Table I are shown such intervals of temperature (ΔT), the shrinkage ($\Delta L/Lo$) attained at these temperatures, and the calculated activation energies (Q). For both temperature ranges, in air as well as in oxygen atmospheres, the solid state densification by diffusion

TABLE I Activation enthalpies calculated using CHR models corresponding to the initial stage sintering of 123

pO_2	$\Delta L/Lo$	ΔT	Q_B^{ini}(kJ/mol)	Q_V^{ini} (kJ/mol)
0.21 atm	0.3–1.7%	827–894°C	612	373
0.21 atm	1.8–2.9%	902–920°C	1800	1510
1 atm	0.2–1.6%	823–908°C	790	502
1 atm	1.8–3.1%	914–934°C	1480	1140

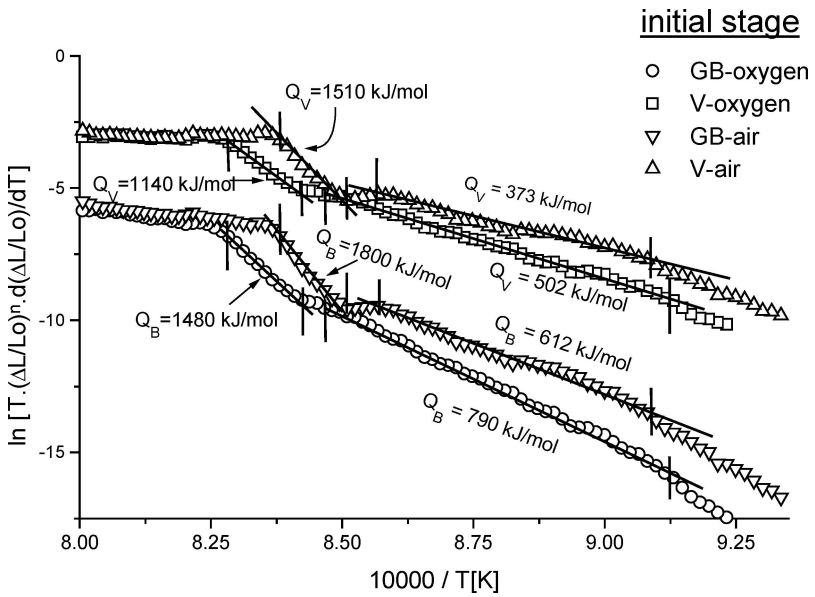

Figure 3 Fittings according to models developed for the initial stage sintering of 123 compacts.

through the volume or lattice exhibits the lowest activation energies.

The ln[function $(\Delta L/Lo, d(\Delta L/Lo)/dT, T)$] curves associated to the densification of 123 compacts in air atmosphere are shown in Fig. 4. These curves are fitted by different densification models: solid state diffusion by grain boundary (Equation 3) and by volume (Equation 4) during the intermediate state of sintering, densification by viscous flow (Equation 5a) and by liquid phase sintering (Equations 5b and 6). Similar fitting-curves were obtained on 123 compacts densified under oxygen flow.

As it is observed in Fig. 4, four zones are fitted by straight lines. The first of them overlaps the zone fitting corresponding to the initial stage sintering models from 900 to 920°C (see Fig. 3). From 920 to 970°C only the curve associated to SP (solution-precipitation) model results with a $Q > 0$. Finally, from 970°C both densification mechanisms, the viscous flow and the solid state diffusion, compete with the solution-precipitation process up to 995°C. Then, the grain boundary diffusion and viscous flow fittings show the lowest activation enthalpy up to 1013°C. Table II lists the activation enthalpy values (Q), the temperature intervals (ΔT) and the shrinkage (ΔL/Lo) where the fittings, using the models associated to intermediate stage sintering mentioned above, are valid.

Similarly, in Table III are quoted the Q values obtained after linear fittings of the dilatometric curves obtained under O_2 flow (not shown here). When the sintering process is driven under oxygen it can also be characterized by four sintering zones, one prior

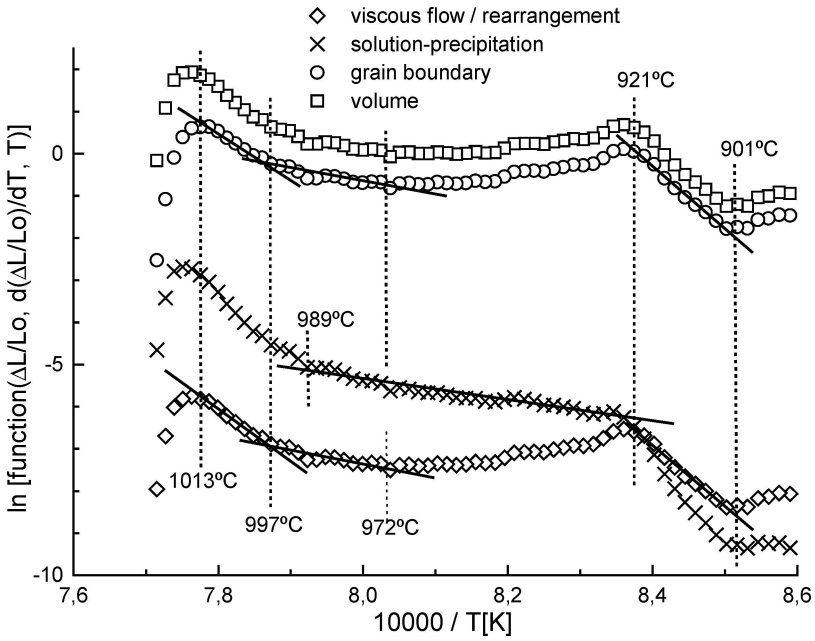

Figure 4 Fitting curves for 123 compacts in air according to theoretical models for the intermediate stage: sintering by solid state diffusion, densification by viscous flow, and sintering assisted by liquid phase.

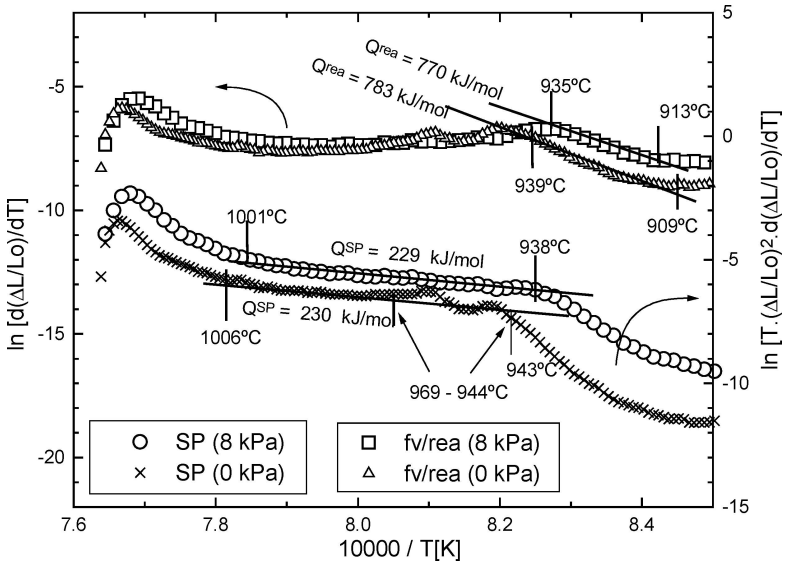

Figure 5 Fitting curves corresponding to liquid phase sintering models of 123-O_2 compacts. Left y-axis: fv/rea mechanisms and right y-axis: SP model.

and subsequent to SP mechanism. As it is noted in Tables I–III all sintering regions are shifted ∼10–20°C towards higher temperatures when the sintering atmosphere is changed from static air to oxygen flow.

TABLE II Activation enthalpies calculated during the intermediate stage sintering of 123-air

$\Delta L/Lo$	ΔT	Q_{fv}^{rea} (kJ/mol)	Q_B^{int} (kJ/mol)	Q_V^{int} (kJ/mol)	Q_L^{sp} (kJ/mol)
1.8–3.1%	901–921°C	1170	1200	1180	1740
3.3–8.4%	922–989°C	–	–	–	207
7.3–9.1%	972–997°C	253	242	305	500
9.0–12.1%	995–1013°C	931	798	1040	1390

TABLE III Activation enthalpies calculated during the intermediate stage sintering of 123 under oxygen flow

$\Delta L/Lo$	ΔT	Q_{fv}^{rea} (kJ/mol)	Q_B^{int} (kJ/mol)	Q_V^{int} (kJ/mol)	Q_L^{sp} (kJ/mol)
1.7–3.2%	913–935°C	770	787	787	1440
3.6–7.9%	938–1001°C	–	–	–	229
8.0–9.6%	990–1014°C	260	249	281	514
9.7–12.6%	1015–1027°C	1390	1110	1440	2020

Other fittings of shrinkage-curves for 123-O_2 compacts are shown in Fig. 5, where there were used both the rearrangement (fv/rea, Equation 5b) and the solution-precipitation models (SP, Equation 6).

In this figure are observed two small peaks between 944–969°C in the fitting curves corresponding to the free sintering (0 kPa). These peaks, attributed to the e1/e2 eutectic reactions, are not detected in load sintering allowing to perform an enlarged linear fitting of the dilatometric curves when a pressure (8 kPa) was exerted on the samples. In any case, and as it can be observed from the fittings in Fig. 5, the differences between the Q values obtained from load sintering (Q^{sp} = 229 kJ/mol, Q^{rea} = 770 kJ/mol) and those from free sintering (Q^{sp} = 230 kJ/mol, Q^{rea} = 783 kJ/mol) are negligible. It is then noted that the Q values in both Tables II and III were calculated from fittings of the load sintering curves.

The 123 microstructures at 940 and 990°C under pO_2 = 1 atm, are shown in Figs 6a and b, respectively. A clear change in both, the size and the shape of 123 grains, is observed when the temperature is increased. Both samples were heated at 5°C/min to the selected temperature and then quenched after given annealing times.

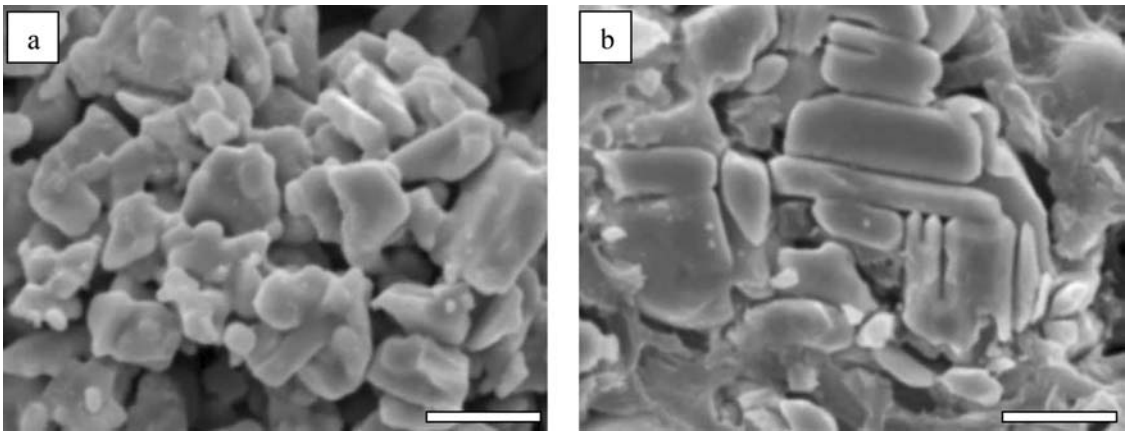

Figure 6 SEM photographs of 123 samples heated at 5°C/min under pO_2 = 1 atm up to (a) 940°C and (b) 990°C. Bar = 5 μm.

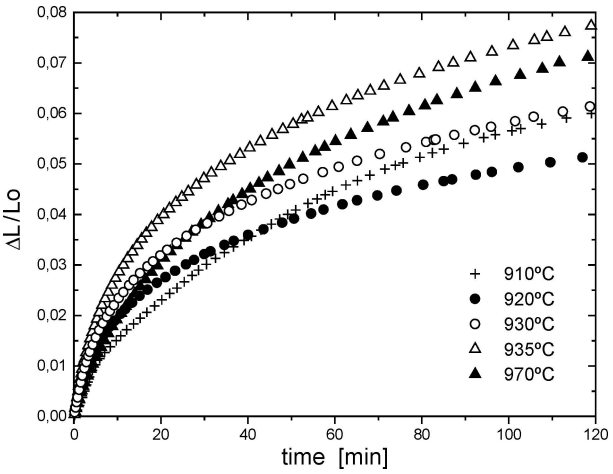

Figure 7 Isothermal dilatometries of 123 compacts in air.

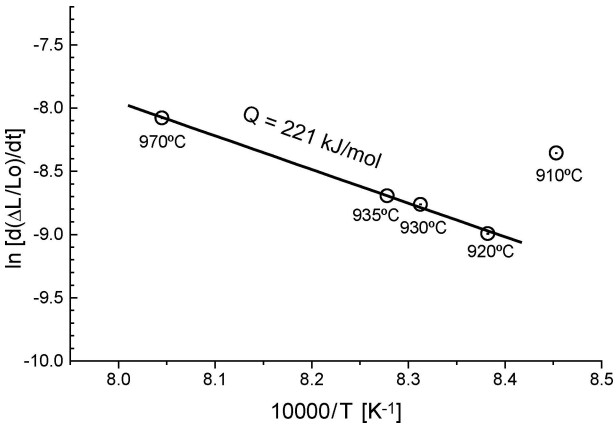

Figure 8 Arrhenius plots from shrinkage rates of 123 (in air) at different constant temperatures.

The 123 grains at 940°C have equiaxial shape and sizes smaller than 5 μm (Fig. 6a), while at 990°C there is some evidence that the 123 suffered grain growth. At 990°C the ceramic grains have changed their equiaxial shape to disk-like and some grains had their longer face larger than 10 μm (Fig. 6b). Therefore, it is noted an important increase in grain growth rate for 123 under oxygen by increasing the temperature from 940 to 990°C.

3.2. Isothermal densification behavior between 910–970°C in air

The contractions of 123 compacts heated in air and maintained at constant temperature (ISO dilatometries) in the range 910–970°C are shown in Fig. 7. These curves were obtained with the pushrod exerting a constant pressure of 8 kPa on the samples.

In these curves Lo is the length of sample at the start of the isothermal cycle, i.e. at $t = 0$. Such data can be interpreted following a previous work by Poisl and Chaklader [33] who calculated the activation energy associated to the sintering process of 123 using an Arrhenius law applied to shrinkage rate:

$$d(\Delta L/Lo)/dt = K \cdot \exp(-Q/RT) \qquad (10)$$

The shrinkage rates were calculated from the ISO curves (Fig. 7) and such values are shown in Table IV. There were selected the $d(\Delta L/Lo)/dt$ values corresponding to the range $t = 80 - 120$ minutes because in this time interval the shrinkage rates had constant values.

Straight lines should be obtained from ln $d(\Delta L/Lo)/dt$ vs. $(1/T)$ plots if Equation 10 applies, and their slopes would be equal to $-Q/R$. As it is observed in Fig. 8, between 920 and 970°C, the values can be fitted by a straight line resulting in $Q =$ 221 kJ/mol. The value corresponding to 910°C is excluded from this line. For this temperature probably a mechanism with a different activation energy than that in the range 920–970°C operates. Further, from Fig. 1 it is apparent this T is in a region of increasing densification rates, whereas for the 920–970°C range such rates decrease monotonically.

Using the ISO dilatometries it is possible to know the main sintering process calculating the n-value from the following contraction-time relationship:

$$\Delta L/Lo = K'.t^n \qquad (11)$$

Plotting $\ln(\Delta L/Lo)$ vs. $\ln(t)$, as shown in Fig. 9, then the n values may be estimated. For the isothermal treatments at $T = 920$, 930, and 935°C the exponent n are 0.33, 0.34, and 0.35, respectively (fitted between 30–130 min), leading to the following expression: $\Delta L/Lo = K' \cdot t^{1/3}$. Such time exponent is characteristic of densification driven by the solution-precipitation process (SP), as proposed by Kingery [27]. However, this exponent takes a value 0.43 at 970°C which differs from the $t^{1/3}$ behavior.

4. Discussion

The activation energy in the 930–955°C range determined on 123 samples by Poisl and Chaklader [33] using isothermal dilatometries in air was 176 ± 12 kJ/mol. A solid state sintering was postulated in that work instead of a solution-precipitation mechanism as it is postulated in our work ($n = 1/3$) with $Q = 221$ kJ/mol. In a more recent work by Imayev *et al.* [12] it was established that the grains grow in the 123-system, characteristic for the intermediate stage of sintering, *starting* from about 900°C and this fact is associated to e1/e2 eutectic reactions. This is coincident with our result

TABLE IV Values of shrinkage rate at different temperatures

Temperature	910°C	920°C	930°C	935°C	970°C
$d(\Delta L/Lo)/dt$	23.5×10^{-5}	12.4×10^{-5}	15.7×10^{-5}	16.8×10^{-5}	31.0×10^{-5}

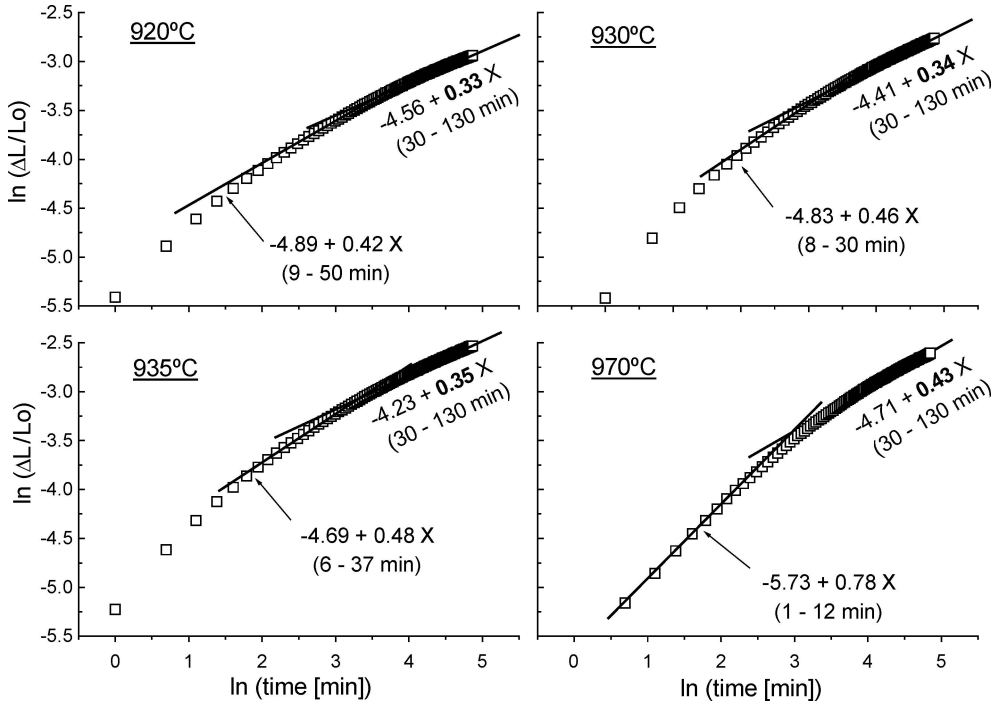

Figure 9 Ln-ln plots to determine the time exponent n.

exposed in the previous section, where it is postulated the liquid phase sintering from 901°C by rearrangement process.

From the Q values obtained for 123-air, it is observed that the solid state diffusion models (corresponding to the intermediate stage of sintering) present a lower activation energy in the 900–920°C range as compared to that for the initial stage of sintering (see Tables I and II). Thus, the volume diffusion mechanism gives a lower Q in this range ($Q_V^{\text{int}} = 1180$ kJ/mol). However, the theoretical model associated to the rearrangement of ceramic grains due to the presence of liquid phase (Equation 5b) present a $Q_L^{\text{rea}} = 1170$ kJ/mol showing that this mechanism would be simultaneously acting with that for volume diffusion. Because the next sintering interval, from about 920 to 970°C, is dominated by SP mechanism, as it is indicate by the Kingery's model, the previous validity of the rearrangement process is justified.

The lowest activation energy along the whole sintering process is obtained for the solution-precipitation mechanism ($Q_L^{\text{sp}} = 207$ kJ/mol) that drives the densification between 920–990°C generating the highest contraction level (≈5%) produced by just only one mechanism. However, this mechanism competes with grain boundary diffusion ($Q_B^{\text{int}} = 242$ kJ/mol; intermediate stage) and viscous flow densification ($Q_{\text{fv}} = 253$ kJ/mol) process from about 970°C. Finally, and prior to 123 peritectic decomposition, for the range 995–1013°C the last two mechanisms compete with activation energies between 800 and 930 kJ/mol.

According to the shrinkage behavior of 123-air at constant temperature $\Delta L/Lo \propto t^{1/3}$ at $T = 920$, 930, and 935°C; thus the SP process could be controlled by a diffusion mechanism. On the other hand, at $T = 970$°C is $\Delta L/Lo \propto t^{\sim 1/2}$ indicating that the SP process could be controlled by interface reaction [27]. However, it is probable that at this temperature other mechanisms, together with SP process, are controlling $YBa_2Cu_3O_{7-x}$ densification as it can be seen from Table II, where Q_{fv}, Q_B^{int} and Q_V^{int} values are comparable to Q_L^{sp} value for 972°C. Then, it may be noted after applying the models based in CHR-dilatometries, as well as in ISO-dilatometries, it is suggested the densification mechanism of 123 compacts in the interval 920–970°C (in air) is the solution-precipitation process. Around 7% difference in the activation energy values, 207 kJ/mol (CHR) and 221 kJ/mol (ISO), is found among the two methods.

It is important to mention the work of Pathak *et al.* [3], who performed isothermal dilatometries on $123/Ag_x$ compacts (x from 0 to 1.2). In the case $x = 0$ (123 alone) they fitted the shrinkage curves in the range 930–985°C obtaining a $Q = 1601$ kJ/mol with a time exponent $n = 0.50$. In our work this range is driven by SP mechanism ($n = 0.33$) and $Q = 221$ kJ/mol. Therefore, the Q values calculated in [3] are greater than those calculated by Poisl and Chaklader [33] and those in this work. These differences in n and Q can be attributed to the fact that Pathak *et al.* [3] considered the contraction curve prior to isothermal cycle converting the time t during nonisothermal contraction to a time t' required to produce the same contraction at that isothermal temperature. This change $t \rightarrow t'$ will modify both the Q and the n values relative to our calculations.

As it was noted above, around 990°C the 123 densification is driven by both grain boundary diffusion and viscous flow. The last one is associated to the densification of amorphous (non crystalline) materials, at first no applicable to $YBa_2Cu_3O_{7-x}$ system. However, it can be interpreted as if the 123 grains were losing their crystalline identity and therefore deforming via

viscous flow. This temperature of 990°C corresponds well to the separation from the base line of the DTA curve at 987°C. Though the 123-system decomposition temperature was determined by DTA at a higher temperature (≈1010°C), it is evident that the peritectic decomposition begins really during this "softening" stage starting at ∼990°C.

From the data in Tables II and III (from CHR dilatometric runs) and assuming that the model giving the lowest activation energy, for a given range ΔT, would be the principal operating mechanism in such ΔT-range, the following conclusions may be advanced. The porous ceramic 123 pellet under air atmosphere densifies initially, ΔT = 827–894°C, by solid state sintering (SSS; initial stage) driven by volume diffusion, Q_V^{ini} = 373 kJ/mol. Then, from 901 to 921°C the formation of a liquid phase, $Q_{\text{fv}}^{\text{rea}}$ = 1170 kJ/mol, appears to compete with densification due to grain growth (GG; intermediate stage) densification, with both grain boundary and volume diffusion operating. In fact in Equations 3 and 4, the quoted Q_B^{int} and Q_V^{int} correspond to the difference $Q_B^{\text{int}} = (Q_B - Q_{\text{GG}})$ or $Q_V^{\text{int}} = (Q_V - Q_{\text{GG}})$, where Q_B or Q_V and Q_{GG} are respectively the Q for densification due to grain growth (intermediate stage in SSS) and the Q for the grain growth mechanism itself (see the assumptions in [23] concerning the derivations of Equations 3 and 4). According to this, the Q_B or Q_V would be much larger than the measured Q_B^{int} or Q_V^{int} (1200 and 1180 kJ/mol) suggesting that in the ΔT range (901–921°C) the main densification is strongly related to the formation of a liquid phase. From 922 to 989°C it is clear that the lowest activation energy is obtained for the solution-precipitation model, giving Q_L^{sp} = 207 kJ/mol. This fact agrees well with both, the conclusions of the isothermal densification analysis and the previous suggestion that a liquid was formed in the 901–921°C range. At the end of the Q_L^{sp} mechanism at ∼989°C, liquid phase rearrangement and/or intermediate stage (GG) densification mechanisms apparently start operating again. These mechanisms are suggested by the obtained energies of $Q_{\text{fv}}^{\text{rea}}$ = 253 kJ/mol and Q_B^{int} = 242 kJ/mol / Q_V^{int} = 305 kJ/mol, in the range 972–997°C. With these relative low values for Q_B^{int} and Q_V^{int}, it seems now more probable the operation of GG mechanisms; this fact would also agree with the well-known tendency for 123 ceramics to show higher grain growth for higher temperatures.

Finally, for the last range up to the peritectic melting of 123 or 011 phases, both mechanisms the viscous flow ($Q_{\text{fv}}^{\text{rea}}$ = 931 kJ/mol) and the grain growth densification (Q_B^{int} = 798 kJ/mol; Q_V^{int} = 1040 kJ/mol) can explain the strong densification measured in the 995–1013°C range (see Fig. 1). On the basis the real Q_B^{int} and Q_V^{int} values are probably even larger, it appears probable either an incipient softening or melting of 123 or 011 phase in the 123 system would drive densification in range 995–1032°C rather than the occurrence of appreciable grain growth at such temperatures. It should be noted such incipient melting would probably be undistinguishable from a densification provided by a creep law whereby the compressed ceramic near its melting point may deform at a strain rate [34] probably given by $d\varepsilon/dt \propto D$, with the diffusion coefficient $D = Do \cdot \exp(-Q/RT)$. The latter would give also a linear $\ln(d\varepsilon/dT)$ versus $1/T$ plot as for the assumed simple viscous flow densification regime represented by Equation 5a.

The sintering behavior of 123 under oxygen flow is similar to 123 sintering in air, but now the sintering ranges are displaced ∼10–20°C towards higher temperatures. It is noteworthy that the grains grow after the e1 eutectic reaction at 940°C, generating a liquid which triggers the SP process. It is known that the presence of a liquid phase not only promotes the grain growth process [35] but also produces an increase in the aspect ratio of grains [12, 36]. Thus the 123 elongated grains, seen in Fig. 6b, is indicative that it is developing a liquid phase sintering in the range 940–990°C under O_2 flow, as it is proposed by the considered theoretical models.

It is clear that the action of 8 kPa during 123 load sintering is sufficient to increase from 10 to 15% the maximum value of $\Delta L/Lo$. By this way, a higher contraction in 123 is verified during (i) the rearrangement stage in which densification mechanism corresponds approximately to a viscous flow [27], and (ii) the softening stage where one of the main mechanism proposed is the viscous flow or creep deformation of the somehow porous solid. This behavior in both stages can be expected because the strain rate of crystals by diffusional creep is proportional to the applied stress ($d\varepsilon/dt \propto \sigma$; [34]).

5. Conclusions

A complete interpretation of the main mechanisms driving the densification of $YBa_2Cu_3O_{7-x}$ ceramic under air and oxygen atmospheres was reached applying different theoretical densification models to the dilatometric shrinkage-curves. The activation enthalpies were calculated using these models and they confirmed a very good agreement among dilatometric methods and predictions from DTA-TG data. Densification runs at constant heating rate permitted to determine different sintering stages. The initial stage sintering is driven by solid state sintering between 827–894°C (823–908°C in O_2). Then, in the interval 902–920°C (914–934°C in O_2) an intermediate-grain growth stage, where the volume diffusion gave the lowest activation enthalpy, competes with the rearrangement process associated to the presence of a liquid phase. This last process is justified because the next sintering stage in the range 922–970°C (938–990°C in O_2 flow) can be fitted by the solution-precipitation model with an activation enthalpy of 207 kJ/mol (229 kJ/mol in O_2). In the range 972–995°C (990–1014°C in O_2), the solid state (GG) intermediate stage sintering mechanism and/or viscous flow compete with the solution-precipitation process. Prior to the peritectic melting (996–1013°C in air; 1015–1027°C in O_2) grain growth plus softening of 123 crystalline grains are apparently the main densification mechanisms.

The models applied to isothermal dilatometries in air between 910–970°C confirmed the sintering behavior established from the constant heating rate dilatometries.

The DTA-TG curves showed reactions prior to the peritectic melting of 123 and they were coincident with the temperatures where the contraction rates increased indicating for example a definite densification process was triggered. These reactions were attributed to the presence of eutectic liquids e1/e2, both rich in Ba and Cu.

Acknowledgments

The authors thanks to Mr. Daniel Quattrini and Mr. Carlos Cottaro, from Bariloche Atomic Center, by DTA-TG runs and SEM images, respectively.

References

1. H. C. LING, *J. Mater. Sci*. **25** (1990) 3297.
2. L. C. PATHAK, S. K. MISHRA, P. G. MUKUNDA, M. M. GODKHINDI, D. BHATTACHARYA and K. L. CHOPRA, *ibid*. **29** (1994) 5455.
3. L. C. PATHAK, S. K. MISHRA, D. BHATTACHARYA and K. L. CHOPRA, *J. Mater. Res*. **14** (1999) 4148.
4. J. GUHA, *J. Am. Ceram. Soc*. **71** (1988) C273.
5. N. M. HWANG, Y. K. PARK, H. K. LEE, J. H. HAHN, G. W. BAHNG, K. W. LEE, H. G. MOON and J. C. PARK, *ibid*. **71** (1988) C210.
6. N. YANG, J. KUNG and P. WU, *J. Cryst. Growth* **91** (1988) 439.
7. E. R. BENAVIDEZ, N. QUARANTA, C. J. R. GONZÁLEZ OLIVER, R. CARUSO, O. DE SANCTIS and A. FRATTINI, *Surf. Coat. Technol*. **122** (1999) 24.
8. M. W. SHIN, T. M. HARE, A. I. KINGON and C. C. KOCH, *J. Mater. Res*. **6** (1991) 2026.
9. C. T. CHU and B. DUNN, *ibid*. **5** (1990) 1819.
10. K. NO, J. D. VERHOEVEN, R. W. MCCALLUM and E. D. GIBSON, *IEEE Trans. Mag*. **25** (1989) 2184.
11. F. J. GOTOR, A. R. FERT, P. ODIER and N. PELLERIN, *J. Am. Ceram. Soc*. **78** (1995) 2113.
12. M. F. IMAYEV, D. B. KAZAKOVA, A. N. GAVRO and A. P. TRUKHAN, *Physica C* **329** (2000) 75.
13. C. W. CHENG, A. C. ROSE-INNES, N. McN. ALFORD, M. A. HARMER and J. D. BIRCHALL, *Supercond. Sci. Technol*. **1** (1988) 113.
14. N. McN. ALFORD, W. J. CLEGG, M. A. HARMER, J. D. BIRCHALL, K. KENDALL and D. H. JONES, *Nature* **332** (1988) 58.
15. E. R. BENAVIDEZ, O. DE SANCTIS, J. E. FISCINA and C. J. R. GONZÁLEZ OLIVER, *J. Mat. Sci. Lett*. **19** (2000) 307.
16. E. R. BENAVIDEZ, Ph.D. Thesis (Universidad Nacional de Rosario, June 2001).
17. C. J. R. GONZALEZ OLIVER and E. R. BENAVIDEZ, *Materia* **8** (2003) 283. {http://www.materia.coppe.ufrj.br/sarra/artigos/artigo10281}
18. E. A. OLIBER, E. R. BENAVIDEZ, G. REQUENA, J. E. FISCINA and C. J. R. GONZÁLEZ OLIVER, *Physica C* **384** (2003) 247.
19. W. S. YOUNG and I. B. CUTLER, *J. Am. Ceram. Soc*. **53** (1970) 659.
20. R. L. COBLE, *J. Appl. Phys*. **32** (1961) 787.
21. *Idem.*, *ibid*. **36** (1965) 2327.
22. R. L. COBLE and T. K. GUPTA, in "Sintering and related phenomena" edited by G.C. Kuczynski *et al*. (Gordon and Breach, N.Y., 1967) p. 423.
23. C. GENUIST and J. M. HAUSSONNE, *Ceram. Intern*. **14** (1988) 169.
24. R. L. COBLE, *J. Appl. Phys*. **32** (1961) 793.
25. J. FRENKEL, *J. Phys. (USSR)* **9** (1945) 385.
26. I. B. CUTLER, *J. Am. Ceram. Soc*. **52** (1969) 14.
27. W. D. KINGERY, *J. Appl. Phys*. **30** (1959) 301.
28. C. J. R. GONZÁLEZ OLIVER, J. E. FISCINA, E. A. OLIBER, D. RUSSO and D. A. ESPARZA, *Termochim. Acta* **203** (1992) 353.
29. J. MIZUSAKI, H. TAWAGA, K. HAYAKAWA and K. HIRANO, *J. Am. Ceram. Soc*. **78** (1995) 1781.
30. T. ASELAGE and K. KEEFER, *J. Mater. Res*. **3** (1988) 1279.
31. K. LAY and G. RENLUND, *J. Am. Ceram. Soc*. **73** (1990) 1208.
32. J. E. ULLMAN, R. W. MCCALLUM and J. D. VERHOEVEN, *J. Mater. Res*. **4** (1989) 752.
33. W. H. POISL and A. C. D. CHAKLADER, *J. Am. Ceram. Soc*. **76** (1993) 1177.
34. R. L. COBLE, *J. Appl. Phys*. **34** (1963) 1679.
35. K. W. LAY, *J. Am. Ceram. Soc*. **51** (1961) 373.
36. L. C. STEARNS, M. P. HARMER and H. M. CHAN, *ibid*. **74** (1991) 2175.

Received 4 March 2004
and accepted 11 March 2005